Study of Rheological-Mechanical Properties and Vibration Mechanics Bandgap of Row Pile Foundation

Qiunan Chen*, Zhixin Li, Xiaocheng Huang and Chen Zhang

School of Civil Engineering, Hunan University of Science and Technology, Xiangtan 411201, China
E-mail: qnchen@hnust.edu.cn
**Corresponding Author*

Received 13 April 2023; Accepted 11 May 2023;
Publication 22 June 2023

Abstract

To analyze the rheological and mechanical properties as well as the vibration-mechanical forbidden zone effect of row pile foundations, this paper employs time-dependent modulus to examine the rheological mechanics of soil. Drawing from viscoelastic theory, we derive the expression of deformation modulus in the frequency domain to analyze the frequency dependence of the shear modulus of rheological soils. We construct a continuous medium dynamics model of the pile-soil periodic structure, taking into account soil rheology, and derive the dispersion equation of shear waves in the periodic structure using the multiple scattering method. The band gap characteristics and parameters that influence the law of shear waves in rheological soil-row pile foundations are studied through the analysis of arithmetic cases. The results show that under the loading condition, the zero-frequency shear modulus of soil is larger than the initial modulus value, and the real part of the

European Journal of Computational Mechanics, Vol. 32_1, 31–52.
doi: 10.13052/ejcm2642-2085.3212

shear modulus decreases monotonically with the increase of frequency and finally converges to the initial modulus value; under the unloading condition, the zero-frequency shear modulus of soil is smaller than the initial modulus value, and the real part of the shear modulus increases monotonically with the increase of frequency and finally converges to the initial modulus value; the larger the relaxation time of soil, the faster the convergence rate; the imaginary part of the shear modulus of soil The imaginary part of the soil shear modulus is positive under loading condition and negative under unloading condition, the value of the imaginary part increases and then decreases with increasing frequency and finally converges to 0. The imaginary part reaches the peak at the critical frequency, the larger the relaxation time the smaller the critical frequency, and the peak of the imaginary part is independent of the relaxation time. This study analyzed the dispersion curve of shear waves in a pile-soil periodic structure and found that increasing low-frequency shear wave velocity in rheological soil pile foundation shifts the band gap position to a higher frequency band, resulting in a smaller band gap width than in linear elastic soil. The relaxation time of soil affects the frequency position and width of the band gap, with larger relaxation times resulting in higher frequency positions and smaller widths. Additionally, soil rheology widens the forbidden vibration band gap of the pile periodic structure when the filling rate of the pile foundation is larger.

Keywords: Fluid mechanics, row pile foundation, vibration mechanics, periodic structure, multiple scattering mechanism, elastic wave bandgap.

1 Introduction

The total area of soft ground in China is widely distributed, for example, the red layer type in southwest China accounts for 33% of the total area of the country, about 82 million km^2, which is the most distributed area of soft ground in China. The red layer is mainly soft rock, which is interstratified or laminated, with poor physical and mechanical properties, low strength, easy to soften in water, easy to disintegrate when losing water, rapid weathering in the open air, certain swelling and rheology, and poor engineering performance. For a long time, during the construction of highways, railroads, water conservancy, and hydropower projects, many professionals in rock mechanics have conducted studies on their special physical and mechanical properties, kinetic properties, and engineering characteristics, including weathering

properties [1, 2], disintegration properties [3, 4], swelling properties [5–10], rheological properties [11–17], and mechanical properties of modified fillers of red soft rocks [18–20]. Among which the rheological properties of soils are the most complex, characterizing significant mechanical properties at both microscopic and macroscopic levels.

In addition, with the rapid economic development, various artificial vibration pollution such as traffic and engineering construction is becoming more and more frequent, and setting vibration isolation barriers in the foundation is an effective method for vibration pollution management [21]. Compared with the traditional methods, barrier vibration isolation has the advantages of low cost, not easy to damage, good durability, simple construction, and can be used as part of the structure, thus it is widely used in practical engineering. Vibration isolation barriers are available in various forms, such as empty trenches, filled trenches, and row piles, which are commonly used in engineering. Although the vibration isolation effect of air ditches and filled ditches is better, the setting depth is generally shallow considering the problems of soil stability and project cost. When the incident wave wavelength is long, the empty trench and filling trench can not play an effective vibration isolation effect, at this time, the row pile is a better choice. Many scholars at home and abroad have conducted a lot of experimental studies and numerical analyses on the vibration isolation of row piles. Woods et al. [22] conducted an experimental study on the vibration isolation effect of discontinuous barriers (such as hole columns and pile columns) using holographic photography. Liao et al. [23] conducted a proportional model test on the vibration isolation of pile columns and hole columns in water using the water wave comparison method. Aviles et al. [24] used the wave function Baroomand et al. [25] studied the vibration isolation of pile columns based on a simplified foundation model, but only the vertical vibrations of the foundation and piles were considered in the analysis while the horizontal vibrations were neglected. [26] conducted a computational analysis of the vibration isolation effect of a pile column using a 3D BEM and proposed a method to equate the row of piles to a filled trench based on a composite mechanic's approach. Breaking the conclusion that the diameter of the discontinuous barrier monolith must be larger than 1/6 of the shielded wavelength proposed by Woods et al. Qiu Chang and Gao Guangyun et al. [27] studied the row pile far-field passive vibration isolation problem by using the integral equation method.

For the aspect of vibration mechanical properties of pile-soil periodic structures, early scholars followed the traditional periodic structure theory

and regarded the soil as an ideal linear elastic material. The forbidden band gap and vibration attenuation law of single- or multi-layered soil-row pile-periodic structures were studied. Chen [28] used finite element software to simulate the vibration isolation performance of a four-component cased pile periodic structure. Although the above-mentioned studies have given a great impetus to the application of the periodic structure in foundation vibration reduction, the study only considers the elastic effect of the soil and ignores the rheological effect of the soil, and the defects of the analytical model cause the analysis results are not accurate enough. The rearrangement and skeletal misalignment of soil particles under stress due to relaxation and creep effects in the actual soil have obvious time effects [29, 30]. Based on the Terzaghi one-dimensional consolidation theory, Yuanqiang Cai [31] analyzed the nonlinear asymptotic process of soil stress-strain under cyclic loading under time effect. Zeng Qingyou [32] calculated the long-term settlement of pile foundations in viscoelastic soils using the Mesri creep model considering soil rheology. Ai Zhiyong [33, 34] did a study on the time-varying behavior of layered viscoelastic foundations with piles as well as beams by using a coupled finite-element-boundary element approach. Lijun He [35] used fractional order derivatives to describe the soil rheology and proposed a creep model for viscoelastic soils, and then made an accurate analysis of the time effect of soil stress-strain.

The above study shows that the stress-strain of rheological soils is time-dependent, and corresponding to the frequency domain analysis, the dynamic response of rheological soils must be frequency-dependent. Thus, it can be seen that for pile-soil periodic structures, whether the frequency dependence of soil stress-strain has a significant effect on the band gap characteristics needs to be further investigated.

To investigate the band gap characteristics of the rheological soil-row pile-cycle structure and the influence law of soil rheology. In this paper, the time-dependent modulus is used to describe the soil rheological effect and construct a continuous medium dynamics model of the pile-soil periodic structure. The multiple scattering method is used to derive the dispersion equation of the periodic system. The periodic pile-graph structure in the structure of this paper forms a phonon crystal structure with a circular pile embedded in a square, forming the first Brillouin zone. On this basis, the forbidden vibration band gap of the rheological soil row pile foundation and the influence law of core parameters are further analyzed, and the mechanical model is shown in Figure 1.

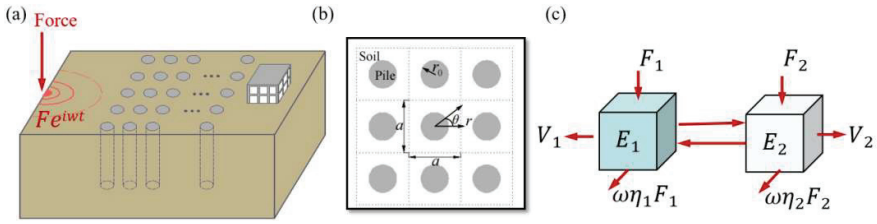

Figure 1 Mechanical analysis model of pile-soil periodic structure (a) Pile-soil dynamics model (b) Bragg two-dimensional analysis plane (c) Micromechanical illustration of soil body.

2 Soil Rheology

The modulus with time dependence is used to describe the rheological effect of the soil, and its integral form of the instanton equation is

$$\sigma^s = \int_{-\infty}^{t} \left[\lambda_s(t-\tau)\delta_{ij}\frac{d\zeta_s}{d\tau} + 2\mu_s(t-\tau)\frac{d\varepsilon^s}{d\tau} \right] d\tau \tag{1}$$

where t is the time variable. ω is the circular frequency. $\boldsymbol{\sigma}^s$ and $\boldsymbol{\varepsilon}^s$ are the stress and strain vectors of the soil body, respectively, δ_{ij} is the Kronecker delta function. ζ_s is the body strain; $\lambda_s = \lambda_s(t)$, $\mu_s = \mu_s(t)$ are Lamé constants, and λ_s, μ_s are functions of time t because of the time dependence of the soil modulus is considered, and τ is the relaxation time.

From the definition of Lamé's constant, it follows that

$$\lambda_s(t) = \frac{E_s(t)v_s}{(1+v_s)(1-2v_s)} \tag{2}$$

$$\mu_s(t) = \frac{E_s(t)}{2(1+v_s)} \tag{3}$$

where v_s is the Poisson's ratio and $E(t)$ is the time-dependent modulus of elasticity. The relaxation function of $E(t)$ takes the form [22]:

$$E_s(t) = E_\infty + (E_0 - E_\infty)e^{-t/\tau} \tag{4}$$

where E_0,

E_∞ is the initial and final steady-state moduli of elasticity, respectively, and e denotes the constant exponential function.

Introducing the Fourier transform of time t to the above equation, the expression in the frequency domain is obtained as

$$E_s(\omega) = E_s^R(\omega) + iE_s^I(\omega) \tag{5}$$

Where ω is the circular frequency and *i* is an imaginary unit, $E_s^I(\omega)$ represent the real and imaginary parts and have:

$$E_s^R(\omega) = \frac{E_\infty + E_0\omega^2\tau^2}{1+\omega^2\tau^2} \tag{6}$$

$$E_s^I(\omega) = \frac{(E_\infty - E_0)\omega\tau}{1+\omega^2\tau^2} \tag{7}$$

The Fourier transform of time *t* is also performed on Equation (1), and the principal equation in the frequency domain is obtained as follows:

$$\sigma^s = \lambda_s(\omega)\delta_{ij}\zeta_s + 2\mu_s(\omega)\varepsilon^s \tag{8}$$

where $\lambda_s(\omega)$, and $\mu_s(\omega)$ are the corresponding Lamé constants in the frequency domain, whose expressions are

$$\lambda_s(\omega) = \frac{\lambda_0(\eta+\omega^2\tau^2)}{1+\omega^2\tau^2} + i\frac{\lambda_0\omega\tau(\eta-1)}{1+\omega^2\tau^2} \tag{9}$$

$$\mu_s(\omega) = \frac{\mu_0(\eta+\omega^2\tau^2)}{1+\omega^2\tau^2} + i\frac{\mu_0\omega\tau(\eta-1)}{1+\omega^2\tau^2} \tag{10}$$

where $\lambda_0 = \frac{v_s E_0}{(1+v_s)(1-2v_s)}$, $\mu_0 = \frac{E_0}{2(1+v_s)}$ are the initial Lamé constants; t is the time variable. ω is the circular frequency; The modulus ratio between initial and final states $\eta = E_\infty/E_0$. It can be seen from Equation.

Figure 2 gives the variation law of Lamé constant μs (shear modulus) with frequency for different values of modulus ratio η (μ_0 is taken as 30 MPa), in which Re and Im denote the real and imaginary parts, respectively. The figure shows that when $\eta > 1$, the real part of the shear modulus Re(μ_s) decreases with the increase of frequency from the zero-frequency shear modulus (the shear modulus at frequency 0, i.e., the static shear modulus) and finally converges to μ_0. When $\eta < 1$, it is less than μ_0, and Re(μ_s) increases with the increase of frequency from increasing to μ_0. And when $\eta = 1$, Re(μ_s) does not change with frequency, and its value is constantly equal to μ_0. As can be seen from the figure, the imaginary part of the shear modulus Im(μ_s) > 0 when $\eta > 1$; and Im(μ_s) < 0 when $\eta < 1$; when $\eta = 1$, then Im(μ_s) is constant to 0. When $\eta > 1$, Im(μ_s) increases positively and peaks with the increase of frequency, and then gradually decreases and converges to 0; and when $\eta < 1$, Im (It should be noted that in actual engineering), $\eta > 1$ represents the loading condition (soil is compacted, $\mathrm{E}_\infty > \mathrm{E}_0$), while $\eta < 1$ represents the unloading condition.

The above analysis shows that the static shear modulus of the soil $\mu_s|_{\omega=0}$ and the real and imaginary parts of the shear modulus is closely related to the constant state modulus ratio η, and there exists a critical frequency ω_{cr}, at which the imaginary part of the shear modulus will have a peak $\mathrm{Im}(\mu)_{s\,\max}$. To obtain the quantization results of, ω_{cr} and $\mathrm{Im}(\mu)_{\mathrm{s\,max}}$, Equation (10) is further analyzed analytically. By taking $\omega = 0$ from Equation (10), it is obtained that

$$\mu_s|_{\omega=0} = \eta\mu_0 \tag{11}$$

The above equation shows that the static shear modulus of the soil is only related to the always-state modulus ratio η, and is linearly related.

Using the extremum theorem to calculate the extremum point of the imaginary part of Equation (11), the critical frequency ω_{cr}: is obtained

$$\sigma^s = \lambda_s(\omega)\delta_{ij}\zeta_s + 2\mu_s(\omega)\varepsilon^s \tag{12}$$

Solving the equation then yields (with negative roots rounded off)

$$\frac{\partial Im(\mu_s)}{\partial\omega} = 1 - 2\tau^2\omega^2 = 0 \tag{13}$$

$$\omega_{cr} = \frac{1}{\sqrt{2}\tau} \tag{14}$$

Equation (13) is the critical frequency of the peak of the imaginary part of the shear modulus, and it can be seen that the critical frequency is only related to the relaxation time τ and is inversely proportional. Substituting Equation (14) into the imaginary part of Equation (7), we obtain the critical frequency ω_{cr} corresponding to the peak of the imaginary part of the shear modulus $\mathrm{Im}(\mu)_{s\,\max}$:

$$Im(\mu_s)_{\max} = \frac{\sqrt{2}}{3}\mu_0(\eta - 1) \tag{15}$$

Equation (15) further shows that the peak of the imaginary part of the shear modulus depends entirely on the constant-state modulus ratio η and is independent of the relaxation time.

Figures 3 and 4 show the curves of shear modulus μs versus frequency for different values of relaxation time τ. As can be seen from the figures, the larger τ is, the faster the real part of μs converges to μ0, and the critical frequency ω_{cr} at which the imaginary part reaches its peak is smaller, which is consistent with the law reflected in Equation (10). It should be noted that

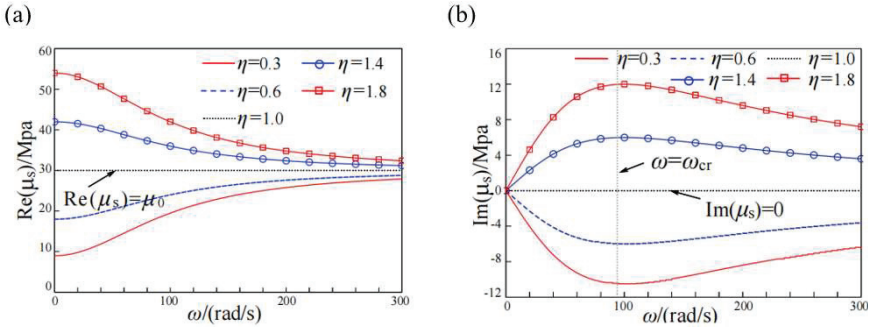

Figure 2 Frequency variation law of shear modulus at $\tau = 1 \times 10^{-2}$ s (a) real part ($\eta = 1.8$) (b) imaginary part ($\eta = 1.8$).

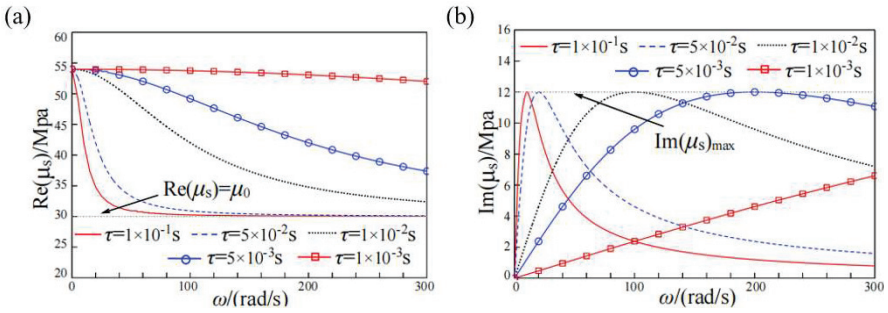

Figure 3 Frequency variation law of shear modulus (a) real part ($\eta = 1.8$) (b) imaginary part ($\eta = 1.8$).

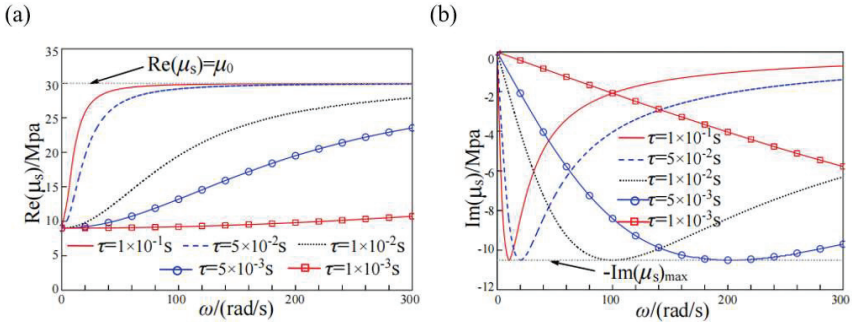

Figure 4 Frequency variation law of shear modulus (a) real part ($\eta = 0.3$) (b) imaginary part ($\eta = 0.3$).

from Equation (7), it can be seen that when $\tau = 0$, the real part of μs will be constantly equal to $\eta\mu 0$, while the imaginary part is constant 0. At this time, the soil degenerates into a linear elastic material.

3 Wave Mechanics Equation

Based on the theory of elastic fluctuations, write the Navier vibration mechanics equations for the soil and pile foundation in the frequency domain as follows:

$$(\lambda_s + \mu_s)\nabla(\nabla \cdot \boldsymbol{u}^s) + \mu_s \nabla^2 \boldsymbol{u}^s + \rho_s \omega^2 \boldsymbol{u}^s = 0 \tag{16}$$

$$(\lambda_p + \mu_p)\nabla(\nabla \cdot \boldsymbol{u}^p) + \mu_p \nabla^2 \boldsymbol{u}^p + \rho_p \omega^2 \boldsymbol{u}^p = 0 \tag{17}$$

Where, $\boldsymbol{u}^s$, $\boldsymbol{u}^p$, ρ_{s}, ρ_{p} are the displacement vector and density of soil and pile foundation respectively; unlike rheological soil, pile foundation is a homogeneous elastic material and its Lamé constants λ_{p}, μ_{p} are constants.

Introducing the potential function, $\boldsymbol{\psi}_{\mathrm{s}}$ the Helmholtz decomposition of the displacement vector $\boldsymbol{u}^{\mathrm{s}}$ of the soil body in the polar coordinate system yields:

$$u_r^s = \frac{\partial \phi_s}{\partial r} + \frac{1}{r}\frac{\partial \psi_s}{\partial \theta} \tag{18}$$

$$u_\theta^s = \frac{1}{r}\frac{\partial \phi_s}{\partial \theta} - \frac{\partial \psi_s}{\partial r} \tag{19}$$

Substituting Equation (18) into Equation (19), we obtain:

$$\begin{cases} \nabla^2 \phi_s + k_{l1}^2 \phi_s = 0 \\ \nabla^2 \psi_s + k_{t1}^2 \psi_s = 0 \end{cases} \tag{20}$$

Where $k_{l1} = \omega / c_{l1}$, $k_{t1} = \omega / c_{t1}$ are the wave numbers of compressional and shear waves in the soil, respectively, and c_{l1}, c_{t1} is the wave velocities of the two waves. It is possible to obtain:

$$\begin{cases} \sigma_r^s = \lambda_s(\omega)\nabla^2 \phi_s + 2\mu_s(\omega)\dfrac{\partial}{\partial r}\left(\dfrac{\partial \phi_s}{\partial r} + \dfrac{1}{r}\dfrac{\partial \psi_s}{\partial \theta}\right) \\ \sigma_{r\theta}^s = \mu_s(\omega)\left(\dfrac{2}{r}\dfrac{\partial^2 \phi_s}{\partial r \partial \theta} - \dfrac{2}{r^2}\dfrac{\partial \phi_s}{\partial \theta} + \dfrac{1}{r^2}\dfrac{\partial^2 \psi_s}{\partial \theta^2} - \dfrac{\partial^2 \psi_s}{\partial r^2} + \dfrac{1}{r}\dfrac{\partial \psi_s}{\partial r}\right) \end{cases} \tag{21}$$

Similarly, the Helmholtz decomposition of the pile fluctuation equation by introducing the potential functions, $\boldsymbol{\psi}_{\mathrm{p}}$ yields

$$\begin{cases} \nabla^2\phi_p + k_{l2}^2\phi_p = 0 \\ \nabla^2\psi_p + k_{t2}^2\psi_p = 0 \end{cases} \tag{22}$$

$$\begin{cases} \sigma_r^p = \lambda_p\nabla^2\phi_p + 2\mu_p\dfrac{\partial}{\partial r}\left(\dfrac{\partial\phi_p}{\partial r} + \dfrac{1}{r}\dfrac{\partial\psi_p}{\partial\theta}\right) \\ \sigma_{r\theta}^p = \mu_p\left(\dfrac{2}{r}\dfrac{\partial^2\phi_p}{\partial r\partial\theta} - \dfrac{2}{r^2}\dfrac{\partial\phi_p}{\partial\theta} + \dfrac{1}{r^2}\dfrac{\partial^2\psi_p}{\partial\theta^2} - \dfrac{\partial^2\psi_p}{\partial r^2} + \dfrac{1}{r}\dfrac{\partial\psi_p}{\partial r}\right) \end{cases} \tag{23}$$

Where k_{l2} and k_{t2} are the wave numbers of compressional and shear waves in the pile foundation.

According to the elastic wave scattering theory [25], the potential functions, ψ_{s}, ψ, ψ_{p} of the soil and pile are expanded by the column wave function to obtain:

$$\begin{cases} \phi_s = \displaystyle\sum_{m=-\infty}^{\infty}[A_{m1}J_m(k_{l1}r) + B_{m1}Y_m(k_{l1}r)]e^{im\theta} \\ \psi_s = \displaystyle\sum_{m=-\infty}^{\infty}[A_{m2}J_m(k_{t1}r) + B_{m2}Y_m(k_{t1}r)]e^{im\theta} \\ \phi_p = \displaystyle\sum_{m=-\infty}^{\infty}C_{m1}J_m(k_{l2}r)e^{im\theta} \\ \psi_p = \displaystyle\sum_{m=-\infty}^{\infty}C_{m2}J_m(k_{t2}r)e^{im\theta} \end{cases} \tag{24}$$

Where, A_{m1}, A_{m2}, B_{m1}, B_{m2}, C_{m1}, and C_{m2} are the pending integration constants, determined by the pile-soil interface conditions; J_{m}, Y_{m} denote the first and second class Bessel functions of order m, respectively, and m is an integer.

The main computational boundary conditions in this paper are free periodic boundary conditions, which are the basis for computing periodic structures/phonon crystals. Substituting into Equation (24), the expressions for the levels of the displacement and stress fields of the soil and pile

foundations are obtained as follows

$$\begin{aligned}
\begin{bmatrix} u_r^s \\ u_\theta^s \end{bmatrix} &= \sum_{m=-\infty}^{+\infty} e^{im\theta} \left\{ \boldsymbol{F}_m \begin{bmatrix} A_{m1} \\ A_{m2} \end{bmatrix} + \boldsymbol{G}_m \begin{bmatrix} B_{m1} \\ B_{m2} \end{bmatrix} \right\} \\
\begin{bmatrix} \sigma_r^s \\ \sigma_{r\theta}^s \end{bmatrix} &= \sum_{m=-\infty}^{+\infty} e^{im\theta} \left\{ \boldsymbol{f}_m \begin{bmatrix} A_{m1} \\ A_{m2} \end{bmatrix} + \boldsymbol{g}_m \begin{bmatrix} B_{m1} \\ B_{m2} \end{bmatrix} \right\} \\
\begin{bmatrix} u_r^p \\ u_\theta^p \end{bmatrix} &= \sum_{m=-\infty}^{+\infty} e^{im\theta} \boldsymbol{D}_m \begin{bmatrix} C_{m1} \\ C_{m2} \end{bmatrix} \\
\begin{bmatrix} \sigma_r^p \\ \sigma_{r\theta}^p \end{bmatrix} &= \sum_{m=-\infty}^{+\infty} \boldsymbol{d}_m e^{im\theta} \begin{bmatrix} C_{m1} \\ C_{m2} \end{bmatrix}
\end{aligned} \tag{25}$$

where the coefficient matrices $\boldsymbol{F}_m$, $\boldsymbol{G}_m$, $\boldsymbol{f}_m$, $\boldsymbol{g}_m$, $\boldsymbol{D}_m$, $\boldsymbol{d}_m$ are known second-order matrices, and their specific expressions are shown in the Appendix.

From the displacement continuity and stress continuity at the pile-soil interface $(r = r_0)$, the interface conditions are obtained as follows:

$$\begin{gathered}
u_r^s = u_r^p,\ u_\theta^s = u_\theta^p,\ \sigma_r^s = \sigma_r^p,\ \sigma_{r\theta}^s = \sigma_{r\theta}^p, \\
\lim{}^{+} x = \lim{}^{-} x
\end{gathered} \tag{26}$$

Substituting Equation (20) into Equation (21), the relationship between the coefficients to be determined A_{m1}, A_{m2}, and B_{m1}, B_{m2} can be organized as follows

$$\begin{bmatrix} A_{m1} \\ A_{m2} \end{bmatrix} = \boldsymbol{P}_m \begin{bmatrix} B_{m1} \\ B_{m2} \end{bmatrix} \tag{27}$$

The soil displacement can be further written as

$$\begin{bmatrix} u_r^s \\ u_\theta^s \end{bmatrix} = \sum_{m=-\infty}^{+\infty} e^{im\theta} \boldsymbol{Q}_m \begin{bmatrix} B_{m1} \\ B_{m2} \end{bmatrix} \tag{28}$$

where $\boldsymbol{P}_m$ and $\boldsymbol{Q}_m$ are known second-order matrices and their expressions are given in the Appendix.

To derive the dispersion equations for the pile-soil periodic structure, the soil displacements in the polar coordinate system need to be converted to the right-angle coordinate system (x-y) of the metric system with the following

conversion relations:

$$\begin{bmatrix} u_x^s \\ u_y^s \end{bmatrix} = \begin{bmatrix} \cos\theta & -\sin\theta \\ \sin\theta & \cos\theta \end{bmatrix} \begin{bmatrix} u_r^s \\ u_\theta^s \end{bmatrix} = \sum_{m=-\infty}^{+\infty} e^{im\theta} \bar{\boldsymbol{Q}}_m \begin{bmatrix} B_{m1} \\ B_{m2} \end{bmatrix} \tag{29}$$

where.

Express the normal displacement on the four boundaries of the beta cell in Figure 1c as

$$\frac{\partial}{\partial \boldsymbol{n}} \begin{bmatrix} u_x^s \\ u_y^s \end{bmatrix}_{\boldsymbol{\Gamma}} = \boldsymbol{\Omega} \begin{bmatrix} u_x^s \\ u_y^s \end{bmatrix}_{\boldsymbol{\Gamma}} \tag{30}$$

where $\boldsymbol{\Gamma} = [\Gamma_1, \Gamma_2, \Gamma_3, \Gamma_4]$ denotes the four boundaries of the beta cell, $\boldsymbol{n} = [n_x, n_y, -n_x, -n_y]$ is the unit normal vector corresponding to the four boundaries; the coefficient matrix $\boldsymbol{\Omega}$ is a matrix of order 8N $\times$ 8N whose matrix elements consist of the matrix elements of $\bar{\boldsymbol{Q}}_m$ and N is the number of computational points selected on each boundary. $\boldsymbol{\Omega}$ corresponds to the matrix elements as follows:

$$\boldsymbol{\Omega} = \boldsymbol{\Omega}_2 \boldsymbol{\Omega}_1^{-1} \tag{31}$$

Among them:

$$\begin{aligned} (\boldsymbol{\Omega}_1)_{jk} &= [\bar{\boldsymbol{Q}}_{k-1-2N}(r_j, \theta_j)] \ldots \\ (\boldsymbol{\Omega}_2)_{jk} &= \frac{\partial}{\partial \boldsymbol{n}} [\bar{\boldsymbol{Q}}_{k-1-2N}(r_j, \theta_j)],\ j,\ k = 1, 2 \ldots 4\mathrm{N}. \end{aligned}$$

According to the Bloch-Floquet theorem, all field quantities $\boldsymbol{\Phi}$ in the periodic structure satisfy the following periodic condition:

$$\boldsymbol{\Phi}(\boldsymbol{X} + a) = \boldsymbol{\Phi}(\boldsymbol{X}) e^{i\boldsymbol{k}a} \tag{32}$$

where $\boldsymbol{X} = [x, y]$ is the coordinate vector and $\mathrm{k} = [\mathrm{k_x}, \mathrm{k_y}]$ is the wave vector.

Applying the period condition (27) to the displacements on the beta cell boundary, we obtain:

$$\begin{aligned} \begin{bmatrix} u_x^s \\ u_y^s \end{bmatrix}_{\Gamma 3} &= e^{ik_y a} \begin{bmatrix} u_x^s \\ u_y^s \end{bmatrix}_{\Gamma 1} \quad \& \\ \begin{bmatrix} u_x^s \\ u_y^s \end{bmatrix}_{\Gamma 4} &= e^{ik_x a} \begin{bmatrix} u_x^s \\ u_y^s \end{bmatrix}_{\Gamma 2} \end{aligned} \tag{33}$$

Substituting Equation (33) into Equation (30), the characteristic equation of the pile-soil system is obtained as

$$\begin{bmatrix} \boldsymbol{\Omega}_{31} & \boldsymbol{\Omega}_{32} \\ \boldsymbol{\Omega}_{41} & \boldsymbol{\Omega}_{42} \end{bmatrix} \begin{bmatrix} \boldsymbol{u^s}|_{\Gamma 1} \\ \boldsymbol{u^s}|_{\Gamma 2} \end{bmatrix} = \begin{bmatrix} \mathbf{M}_{11} & \mathbf{M}_{12} \\ \mathbf{M}_{21} & \mathbf{M}_{22} \end{bmatrix} \begin{bmatrix} \boldsymbol{u^s}|_{\Gamma 1} \\ \boldsymbol{u^s}|_{\Gamma 2} \end{bmatrix} \tag{34}$$

where $\boldsymbol{\Omega}_{31}$, $\boldsymbol{\Omega}_{32}$, $\boldsymbol{\Omega}_{41}$, $\boldsymbol{\Omega}_{42}$ are the two-dimensional chunk matrices in $\boldsymbol{\Omega}$ and the coefficient matrices $\mathbf{M}_{11}$, $\mathbf{M}_{12}$, $\mathbf{M}_{21}$, and $\mathbf{M}_{22}$ are determined by the following equations:

$$\begin{aligned} \mathrm{M}_{11} &= \boldsymbol{\Omega}_{13} e^{2ik_y a} + (\boldsymbol{\Omega}_{11} - \boldsymbol{\Omega}_{33}) e^{ik_y a} \ldots \\ \mathrm{M}_{12} &= \boldsymbol{\Omega}_{12} e^{ik_y a} - \boldsymbol{\Omega}_{34} e^{ik_x a} + \boldsymbol{\Omega}_{14} e^{i(k_x + k_y)a} \ldots \\ \mathrm{M}_{21} &= \boldsymbol{\Omega}_{21} e^{ik_x a} + \boldsymbol{\Omega}_{23} e^{i(k_x + k_y)a} - \boldsymbol{\Omega}_{43} e^{ik_y a} \ldots \\ \mathrm{M}_{22} &= \boldsymbol{\Omega}_{24} e^{2ik_x a} + (\boldsymbol{\Omega}_{22} - \boldsymbol{\Omega}_{44}) e^{ik_x a}. \end{aligned}$$

The above equation is further organized into the standard equation form:

$$\begin{bmatrix} T_1 e^{ik_{x,y}a} + T_2 & T_3 \\ -\boldsymbol{I} & \boldsymbol{I} e^{ik_{x,y}a} \end{bmatrix} \begin{bmatrix} \boldsymbol{V} \\ \boldsymbol{U} \end{bmatrix} = 0 \tag{35}$$

The above equation is a matrix equation of order 8N $\times$ 8N, where $\boldsymbol{I}$ is a unit matrix of order 4N $\times$ 4N; $\boldsymbol{U}$ is the displacement matrix on the metric cell boundary, $\boldsymbol{U} = [u_x^s|_{\Gamma 1}, u_y^s|_{\Gamma 1}, u_x^s|_{\Gamma 2}, u_y^s|_{\Gamma 2}]^T$ denotes the transpose of the matrix, and the expressions of the matrices $\mathbf{T}_1, \mathbf{T}_2, \mathbf{T}_3$ are shown in the appendix.

Using the extraordinary solution condition, one obtains:

$$\det \begin{bmatrix} T_1 e^{ik_{x,y}a} + T_2 & T_3 \\ -\boldsymbol{I} & \boldsymbol{I} e^{ik_{x,y}a} \end{bmatrix} = 0 \tag{36}$$

Equation (36) is the dispersion equation for the pile-soil periodic structure, and det denotes taking the determinant. Given an angular frequency ω, the dispersion curves (frequency-wave number relationship) of compressional and shear waves in the periodic system are obtained by searching for wave vectors k_x, k_y in the first integrable Brillouin domain Γ-X-M. Note that for the Γ-X boundary ($0 \leq k_x \leq \pi/\mathrm{a}$), the exponential term in the equation is taken as, $e^{ik_x a}$ and for the X-M ($0 \leq k_y \leq \pi/\mathrm{a}$) boundary, the exponential term is taken as. When calculating the dispersion curves in the

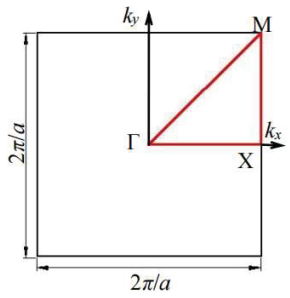

Figure 5 First Brillouin zone in mechanical mode.

text, the number of plane waves m taken should be large enough to ensure the convergence of the results. The exact size taken usually depends on the size and characteristics of the system being simulated. In this paper, the number of plane waves is 101.

4 Analysis of Mechanical Calculations

Firstly, the vibration mechanics solution method and calculation procedure of this paper are verified, and it is known from the previous analysis that the soil model degenerates to a linear elastic model when the relaxation time τ is taken as 0. Figure 6 gives the shear wave dispersion curve on the Γ-X boundary of the degraded model in this paper, and the required computational parameters are taken in Table 1 and compared with the results of the simulation. The normalized dimensionless frequency $f^* = \omega a/(2\pi c_{t2})$

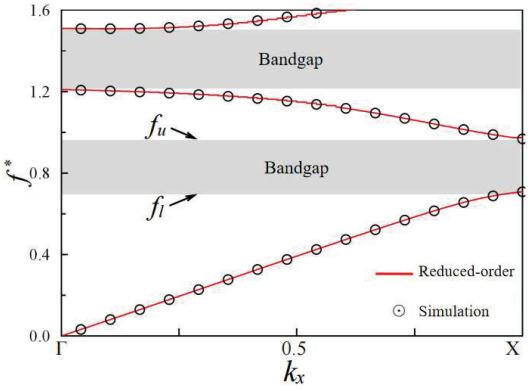

Figure 6 Comparison of mechanical band gap results.

Table 1 Table of mechanical parameters

Density of soil	ρ_{s} (kg-m)$^{-3}$	1900
Initial shear modulus of soil	μ_0 (MPa)	30
Poisson's ratio of soil	υ_{s}	0.25
Density of pile	ρ_{p} (kg-m)$^{-3}$	2500
Lamé constants of pile	λ_{p} (GPa)	8.3
	μ_{p} (GPa)	12.5
Radius of pile	r_0 (m)	0.65
Periodic constant	*an* (m)	2

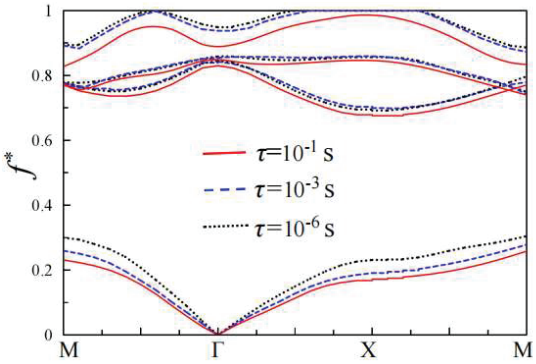

Figure 7 Dispersion curve of shear wave dynamics.

is used as the vertical coordinate in the figure, and the results of both can be found to match by comparison. The shaded area in the figure is the forbidden band gap of the periodic structure, and two band gaps appear in the range of $0 \leq \omega \leq 500$ rad/s. f_u, f_l is the upper and lower bound frequencies of the band gap, respectively. The band gap range in these two parts is mainly due to the bragg scattering effect in the first two orders.

In this paper, the band gap characteristics of shear waves in pile-soil periodic structures are analyzed. Figures 7 and 8 give the dispersion curves of shear waves in the periodic structure when considering the soil rheology. It can be seen that the shear wave velocities in the low-frequency and high-frequency regions increase to different degrees when the relaxation time increases and the increase in the low-frequency region to be significantly larger than that in the high-frequency region, which causes the width of the forbidden band gap to decrease. Figure 7 shows the variation curve of the band gap width W^* with the relaxation time, $W^* = f_u - f_l$. The figure shows that the band gap width decreases gradually with the increase of the

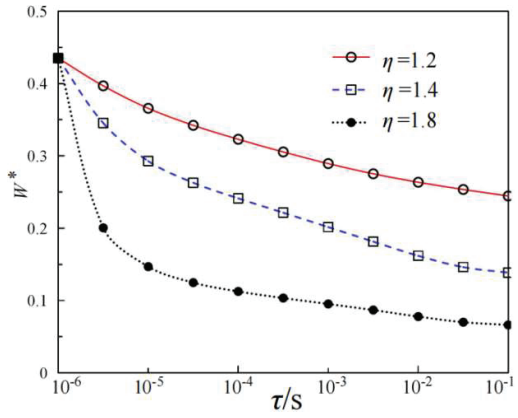

Figure 8 Time-varying curves of the kinetic bandgap width.

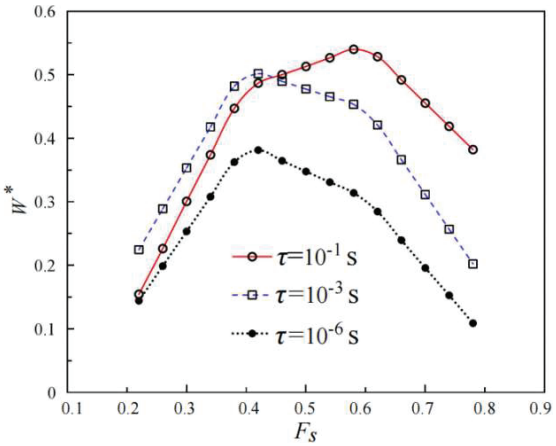

Figure 9 Filling rate variation curve for kinetic band gap width.

relaxation time, and the larger the modulus ratio η, the larger the reduction of the band gap width.

Figure 9 shows the variation curve of band gap width with pile filling rate F_s. The graph shows that the variation curve of band gap width with F_s in the rheological soil pile-periodic structure is similar to that of the elastic soil pile-periodic structure in that the band gap width increases and then decreases as the filling rate increases. At the same filling rate, the band gap width in rheological soil row pile structure is larger than that in linear elastic soil, and the larger the filling rate ($F_s \geq 0.4$), the larger the soil relaxation time is,

the larger the band gap width is. Therefore, when the filling rate of the pile foundation is larger, the soil rheology is beneficial to widen the forbidden band gap of the pile-periodic structure, and the use of large diameter piles has a better vibration isolation effect for rheological soil pile foundations.

5 Conclusion and Discussion

In this paper, the rheology of soil is described using the time-dependent modulus, and the frequency dependence of the shear modulus is analyzed by deriving expressions for the deformation modulus in the frequency domain. The dispersion curves of shear waves in pile-soil periodic structures are then calculated using the multiple scattering method to investigate the band gap characteristics of these waves in more detail. Based on these analyses, several conclusions can be drawn:

(1) When $\eta > 1$ (loading condition), the zero-frequency shear modulus of the soil is greater than the initial modulus value, and the real part of the shear modulus decreases monotonically with the increase of frequency, and finally converges to the initial modulus value. when $\eta < 1$ (unloading condition), the zero-frequency shear modulus of the soil is less than the initial modulus value, and the real part of the shear modulus increases monotonically with the increase of frequency.

(2) The imaginary part of the soil shear modulus is positive during loading and negative during unloading. Its value increases and then decreases with frequency, eventually converging to zero. The peak of the imaginary part occurs at the critical frequency, which decreases as the relaxation time increases. However, the peak value of the imaginary part is independent of the relaxation time. These findings suggest that the frequency dependence of the shear modulus of rheological soils is significant and should be taken into account in soil mechanics and foundation engineering.

(3) The low-frequency shear wave velocity in rheological soil pile foundation increases, so that the band gap position moves to the higher frequency band, and the band gap width is smaller than that of linear elastic soil. The larger the soil relaxation time, the higher the frequency position of the band gap and the smaller the width.

(4) When the filling rate of the pile foundation is larger, the soil rheology is conducive to widening the forbidden vibration band gap of the periodic structure, and the use of large diameter piles has a better vibration isolation effect for rheological soil row pile foundation.

References

[1] Yang Zongcai, Zhang Junyun, Zhou Depei. Study on the rapid weathering characteristics of red-layered mudstone slopes. Journal of Rock Mechanics and Engineering, 2006, 25(2): 275–283.

[2] Zhang J.Y., Zhou D.P. … Rapid weathering law of red-layered mudstone slopes. Journal of Southwest Jiaotong University, 2006, 41(1): 74–79.

[3] Pan Y, Liu Z, Zhou Cuiying. Experiments on water disintegration characteristics of red-bedded soft rock and its interface model. Geotechnics, 2017, 38(11): 3231–3239.

[4] Wu Daoxiang, Liu Hongjie, Wang Guoqiang. Indoor experimental study on the disintegration properties of red-bedded soft rocks. Journal of Rock Mechanics and Engineering, 2010, 29.

[5] Diao X. H., Yang S. X., C. S. B. Experimental study of water absorption and swelling characteristics of mudstone under different temperature and humidity environments. Journal of East China Jiaotong University, 2017, 34(3): 14–18.

[6] Hu WJ, Ding Y, Xia ZY, et al. Experimental study on the lateral limit of the swelling performance of red-layered mudstone in the Chongqing area. Journal of Disaster Prevention and Mitigation Engineering, 2015, 35(5): 607–611.

[7] Ji M, Gao Gao, Gao YN, et al. Study on the time effect of water swelling of ash mudstone. Journal of China University of Mining and Technology, 2010, 39(4): 511–515.

[8] Liu X.L., Wang S.J., Wang E.C., et al. Swelling intrinsic relations of swelling rocks containing time effects. Journal of Water Resources, 2006, 37(2): 195–199.

[9] Wei YX, Zhang SZ, Gan Y, et al. Experimental study on basic properties and swelling and softening of red-bedded mudstone in Sichuan Basin. Engineering Investigation, 2010: 61–68.

[10] Zhong ZB, Li AH, Deng RG, et al. Experimental study on the time-dependent expansion-deformation characteristics of red-bedded mudstone in central Sichuan. Journal of Rock Mechanics and Engineering, 2019, 38(1): 76–86.

[11] Chen Wenwu, Yuan Pengbo, Liu Xiaowei. Experimental study on creep characteristics of red-bedded soft rocks under graded loading conditions. Journal of Rock Mechanics and Engineering, 2009, 28(Suppl. 1): 3076–3081.

[12] Ju Nengpan, Huang Haifeng, Zheng Da, et al. Creep properties of red-bedded mudstone considering water content and improved Burgers model. Geotechnics, 2016, 37: 67–74.
[13] Liu S. W., Chen W. W., Zhang F. Y., et al. Experimental study on rheological properties of Neoproterozoic red-bedded soft rocks. Chinese Desert, 2012, 32(5): 1268–1274.
[14] Wang Yanchao. Study on creep mechanical properties of Badong Formation mudstone and temporal properties of slope deformation and support. Wuhan: China University of Geosciences, 2018.
[15] Yan Yunming, Li Hengle, Guo Shili. Experimental study of triaxial creep mechanical properties of purple-red mudstone. Journal of Changjiang Academy of Sciences, 2017, 34(6): 88–92.
[16] Yang Shu-Bi, Xu Jin, Dong Xiao-Bi. Study on the rheological characteristics of sandy-mudstone interbedded slopes in the red-bedded area. Geological Hazards and Environmental Protection, 1996, 7(2): 12–24.
[17] Jian W, Wang Z, Yin K. Mechanism of the Anlesi landslide in the Three Gorges Reservoir, China. Engineering Geology, 2009, 108(1–2): 86–95.
[18] Wang Zhimeng. Research on red-layered mudstone's adaptability and engineering technology and its improved soil filling for high-speed railroad roadbed [Doctoral dissertation]. Chengdu: Southwest Jiaotong University, 2009.
[19] Wei Y. X. Experimental study on the technology of using red-layered mudstone to fill the roadbed of high-speed railroad. Journal of Railway Engineering, 2009, (12): 39–43.
[20] Yangyang Wei, et al. Bionic Mechanical Analysis of Dragonfly Wings: The Feasibility of Mesh Combination to Improve Structural Stiffness. European Journal of Computational Mechanics, 2022, 31(4): 459–504.
[21] Yang, Xianjian. Geodynamic problems in industrial environmental vibration. Journal of Geotechnical Engineering, 1992, 114(2): 82–88.
[22] Woods R D, Barnet N E, Sangesser R. A new tool for soil dynamics. Journal of Geotechnical Engineering Division, ASCE, 1974, 100(11): 1234–1247.
[23] Liao S, Sangrey D A. Use of piles as isolation barriers. Journal of Geotechnical Engineering Division, ASCE, 1978, 104(9): 1139–1152.
[24] Aviles J, Sanchez-Sesma F J. Piles as barriers for elastic waves. Journal of Geotechnical Engineering, 1983, 109(9): 1134–1146.
[25] Baroomand B, Kaynia A M. Vibration isolation by an array of piles//Soil Dynamics and Earthquake Engineering. southampton: Computational Mechanics Publications, 1991: 683–691.

[26] Kattis S E, Polyzos D, Beskos D E. Vibration isolation by a row of piles using a 3-D frequency domain BEM. International Journal for Numerical Methods in Engineering, 1999, 46(5): 713–728.
[27] Qiu Chang. Three-dimensional Analysis of Far-Field Passive Vibration Isolation for Continuous and Discontinuous Barriers [Doctoral dissertation D]. Shanghai: Tongji University, 2003.
[28] Chen X.B., Wang Y.S., Tang M.X., et al. Characterization of periodic four-component local resonant pile band gap and vibration isolation performance. Geotechnics, 2022, 43(1): 110–118.
[29] Chen, Zongji. One-way problems of consolidation and sub-temporal effects. Journal of Civil Engineering, 1958, 5(1): 1–10.
[30] Wang Taiheng et al. Analysis of Factors Influencing Mechanical Properties of Corrugated Steel Based on Entropy Method. European Journal of Computational Mechanics, 2022, 31(4): 539–554.
[31] Cai Yuanqiang, Liang X, Zheng Zaofeng, et al. One-dimensional consolidation of viscoelastic soil layers with semi-permeable boundaries under cyclic loading. Journal of Civil Engineering, 2003, 36(8): 86–90.
[32] Zeng QY, Zhou J, Qu JT. A method for calculating long-term settlement of pile foundations considering stress-strain time effects. Geotechnics, 2005, 26(8): 1283–1287.
[33] Ai Zhiyong, Wang He Mu, Jin Jing. Timing study of laminar fractional-order viscoelastic saturated foundations acting together with beams. Journal of Mechanics, 2021, 53(5), 1402–1411.
[34] Ai Z Y, Zhao Y Z, Cheng Y C. Time-dependent response of laterally loaded piles and pile groups embedded in transversely isotropic saturated viscoelastic soils. Computers and Geotechnics, 2020, 128: 103815.
[35] He LJ, Kong LW, Wu WJ, et al. A model for describing creep in soft clay using fractional order derivatives. Geotechnics, 2011, 32(S2): 239–243.

Biographies

Qiunan Chen received the bachelor's degree in science from Jinggangshan University in 1987, the master's degree in engineering from Central South University in 1997, and the doctorate degree in engineering from Chongqing University in 2005. He is currently working as an Professor at the Department of Civil Engineering of Hunan University of Science and Technology. His research areas and directions include surrounding rock stability and dynamic construction control of tunnel and underground engineering, consolidation theory and treatment technology of soft soil foundation.

Zhixin Li received the bachelor's degree in engineering from Hunan University of Science and Technology in 2019. He is currently studying as a graduate student at the School of Civil Engineering of Hunan University of Science and Technology. He research areas and directions include geotechnical engineering, foundation pit.

Xiaocheng Huang received the bachelor's degree in engineering from Hunan University of Science and Technology in 2011, the master's degree in engineering from Hunan University of Science and Technology in 2014, and the doctorate degree in engineering from Chongqing University in 2018. He is currently working as an Professor at the Department of Civil Engineering of Hunan University of Science and Technology. His research areas and directions include reliability analysis, risk control theory, prediction of adverse geological disasters in geotechnical engineering.

Chen Zhang received the bachelor's degree in engineering from Chang'an University in 2018. He is currently studying as a graduate student at the School of Civil Engineering of Hunan University of Science and Technology. He research areas and directions include Slope Engineering, geotechnical engineering.